The Microstructure of Electrodeposited Titanium-Aluminum Alloys

G.M. JANOWSKI and G.R. STAFFORD

The microstructure of electrodeposited titanium-aluminide alloys containing 3.6 to 24.1 at. pct Ti was studied by transmission electron microscopy. The surface morphology of the deposits showed that they contained nodular and faceted grains which tended to be less faceted at higher Ti contents. Extensive {111} twinning was observed in all deposits, and growth striations parallel to {111} were observed in the low Ti deposits. The growth of nodules was linked to the presence of these twins; it was hypothesized that the twin boundaries act as easy atomic attachment points and, therefore, enhance the growth rate. The presence of twins and striations was used to propose a growth mechanism. The 5.3, 15.8, and 24.1 at. pct Ti deposits were single-phase grains of the $L1_2$ crystal structure, as opposed to the expected equilibrium two-phase mixture of face-centered cubic (fcc) Al (saturated with Ti) and $D0_{22}$ Al_3Ti. Calculated electron diffraction intensity data were used to demonstrate that the decrease in intensity of the superlattice reflections in the substoichiometric deposits is due to a reduction in the difference in atomic scattering factors between the two lattice site types.

I. INTRODUCTION

MUCH of the research in the area of low-density intermetallic compounds has focused on Al_3Ti-based alloys, with applications envisioned for monolithic and, more likely, composite materials. The materials of interest are ternary or higher order alloys with transition metals, for example, Cu, Ni, Pd, Zn, Mn, or Mo, being added to stabilize the $L1_2$ crystal structure (simple cubic Bravais lattice) rather than the equilibrium binary $D0_{22}$ structure (body-centered tetragonal). This change in crystal structure is considered desirable, since the higher symmetry of the $L1_2$ structure would be expected to increase the number of slip systems, therefore, enhancing toughness and/or ductility. Discussions of slip systems, alloying effects, and mechanical properties have been published for various Al-Ti-X alloys fabricated by casting or powder metallurgy methods.[1–8]

The present study examines the microstructure of Al-Ti alloys with 3.6 to 24.1 at. pct Ti* electrodeposited from a molten chloroaluminate electrolyte. Although the technique of electrodeposition is very different from traditional approaches used to fabricate these alloys, a number of analogies exist between it and rapid solidification. For example, Grushko and Stafford have shown that by using electrodeposition, extended solid solutions, stable and metastable crystalline phases, quasicrystalline phases, and amorphous phases can all be formed in the Al-Mn system.[9–13] Electrodeposition is an attractive method for fabricating intermetallic compounds since (1) high-temperature consolidation is unnecessary, (2) it is a near-net-shape process, (3) undesirable compositional inhomogeneities are very limited in scale, and (4) grain sizes are typically very small. The purpose of this article is to report the electrodeposition of titanium-aluminide intermetallic compounds. In addition, it is shown that these materials have unique microstructural characteristics, such as extended Ti solid solubility, extensive twinning, and a metastable, binary $L1_2$ phase, which are a result of this processing method.

*All compositions will be given in atomic percent.

G.M. JANOWSKI, formerly NIST/NRC Postdoctoral Research Associate, National Institute of Standards and Technology, is Assistant Professor, Department of Materials Science and Engineering, The University of Alabama at Birmingham, Birmingham, AL 35294-4461. G.R. STAFFORD, Research Chemist, is with the Metallurgy Division, National Institute of Standards and Technology, Gaithersburg, MD 20899.

Manuscript submitted October 2, 1991.

II. EXPERIMENTAL PROCEDURE

A schematic of the electrodeposition process which was used to fabricate the materials of this study is shown in Figure 1. The electrochemical cell was made of jacketed PYREX* ** glass. Its temperature was maintained at 150 °C by a Cole-Parmer Model 1268-44 Circulator which continually pumped silicone fluid through the cell jacket. All electrodes were placed through a TEFLON† cap, and an argon purge (99.999 pct, Air Products,Washington, DC) was maintained over the electrolyte at all times. The counter and reference electrodes were aluminum wire (99.998 pct, Morton Thiokol, Inc., Danvers, MA); each was separated from the working compartment by a glass frit. The working compartment contained the following components: (1) a 0.80-mm-diameter tungsten wire sealed in glass and polished (through 0.25 μm diamond) for electroanalytical determination of the Ti^{+2} concentration; (2) a 0.75-mm titanium wire (99.98 pct, Morton Thiokol, Inc.) to be electrochemically dissolved to produce Ti^{+2}; and (3) a 0.80-mm copper wire to serve as the substrate during electrodeposition. The electrolyte was a 2:1 mole ratio of $AlCl_3$:NaCl. The $AlCl_3$ (anhydrous, 99.9 pct) was obtained from Armant Metal Chloride (Vacherie, LA) and was sublimed at 195 °C in the

*PYREX is a trademark of Corning Glass Works, Corning, NY.

**Tradenames are mentioned only for purposes of completeness of the experimental procedure; in no case does their use imply a recommendation or endorsement by the NIST.

†TEFLON is a trademark of E.I. Du Pont de Nemours & Co., Inc., Wilmington, DE.

presence of helium (99.999 pct, Air Products) prior to use. The NaCl (analytical reagent, Mallinckrodt, Paris, KY) was dried for 4 hours at 500 °C. All chemicals were stored in a Vacuum Atmospheres brand dry box containing argon (99.999 pct, Air Products). The powders were thoroughly mixed before being transferred to the cell. Initially, the reference, counter, and working compartments of the electrochemical cell contained electrolyte of identical composition. The working compartment contained 26 ml of molten electrolyte. The volume of electrolyte in the working compartment was sufficiently large (relative to the amount of deposit) that its composition was essentially unchanged during deposition. Ti^{+2} was added to the working compartment by galvanostatic dissolution of titanium metal. In this study, the concentration of the Ti^{+2} ion was varied between 10 and 25 mM.

The copper substrates used in the electrodeposition experiments were electropolished in a 50 pct phosphoric acid/water solution and dried thoroughly. After introduction into the melt, they were allowed to come to thermal equilibrium at a potential of +0.01 V *vs* Al in order to cathodically protect the copper. The deposition process was controlled galvanostatically at 25 mA/cm^2 until a charge of 1 $coulomb/cm^2$ had passed in order to eliminate problems associated with nucleation overpotentials. The current was then adjusted to the value chosen for that electrodeposit. The deposit thickness was controlled by the total charge which was passed through the cell and ranged from 2 to 50 μm.

The surface morphology of the electrodeposits was studied by scanning electron microscopy (SEM). After a room-temperature zincate treatment and cyanide copper strike, the electrodeposits were overplated with bright copper to a total diameter of approximately 5 mm. These bars were sliced to produce cross-sectional specimens which were 0.80-mm-ID rings of titanium-aluminide deposit surrounded by a copper matrix.

The alloy compositions were determined by performing energy dispersive X-ray spectroscopy ((EDS), quantitative analysis) on polished cross sections; elemental aluminum and titanium were used as standards. The reported values are an average of at least four measurements. Based on these compositions, the binary samples were designated A through D in order of increasing titanium content. The specimen designations, Ti^{+2} concentrations, and current density data are contained in Table I.

The crystal structure, grain morphology, and other microstructural features were examined using a 300 kV transmission electron microscope (TEM). The samples were prepared by cold-stage ion milling 50- to 75-μm-thick cross sections which were partially masked and supported with oval-slotted copper disks.

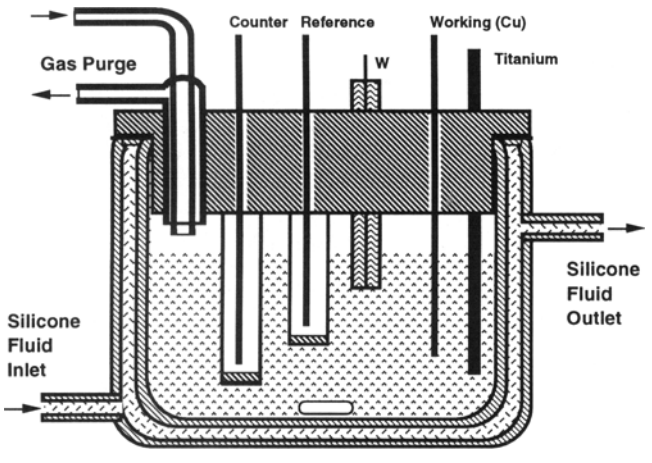

Fig. 1—Schematic of the electrodeposition process. See text for description.

III. RESULTS

A. *Chemical Composition*

Though the exact nature of the deposition process as it relates to alloy composition is not presently understood, it appears that a major factor contributing to alloy composition is whether or not the surface concentration of Ti^{+2} is sufficient to maintain the partial current required for that particular alloy composition.[14] When the Ti^{+2} cation is dilute, there is a significant dependency of alloy composition on current density. A decrease in the titanium content of the deposit is observed with increasing current density as a result of titanium cation depletion at the deposit/electrolyte interface. This dependency is reduced as the Ti^{+2} concentration increases and is virtually eliminated as it approaches 150 mM. At this Ti^{+2} concentration, an alloy containing 25 at. pct Ti is deposited at all current densities less than 40 mA/cm^2. The electroactive aluminum species, $Al_2Cl_7^-$, is not diffusion-limited at these current densities.

The chemical compositions of selected deposits, which were determined by EDS, are shown in Table I. The titanium content of the binary deposits ranged from 3.6 to 24.1 at. pct with the balance being Al. Within the spatial resolution ($\approx$1 μm) and precision limitations of SEM/EDS, the deposits were compositionally homogeneous. A line trace of specimen D, which contains 24.1 at. pct Ti, is shown in Figure 2 and demonstrates that there is no systematic change in composition through the deposit thickness. Additional EDS experiments using a fine electron probe in the TEM, which has a much smaller excitation volume than SEM/EDS ($\approx$0.1 μm), did not show any local changes in chemical composition. It can, therefore, be concluded that within the spatial resolution of these techniques, the Al-Ti electrodeposits characterized in this study are chemically homogeneous.

B. *Surface Morphology*

The surface morphologies of deposits A (3.6Ti) and D (24.1 Ti) are shown in Figure 3. These two specimens

Table I. Deposition Characteristics and Compositions of Al_3Ti-Based Specimens

Sample Designation	Concentration of Ti^{+2} Ions in Electrolyte (mM)	Current Density ($mA \cdot cm^{-2}$)	Deposit Ti Composition (At. Pct)
A	10	6.8	3.6
B	10	2.3	5.3
C	25	30.2	15.8
D	10	0.2	24.1

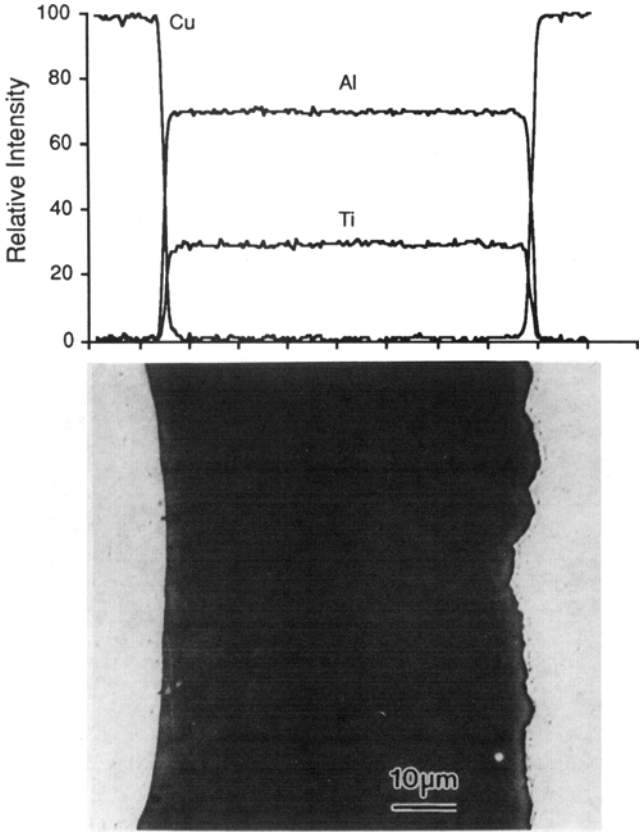

Fig. 2—Polished cross section and SEM/EDS line trace of the 24.1 at. pct Ti deposit which shows the capabilities for compositional uniformity inherent to the electrodeposition process.

are typical of the low Ti and high Ti sample types, respectively. The low Ti specimens comprise nodules that often resemble dendrites; *i.e.*, the deposit surface is not microscopically flat and appears to have formed by crystallographically controlled growth. This surface morphology is similar to that of high-purity Al deposited under similar conditions.[15–18] An increase in the titanium content results in a less dendritic nodular deposit. In all cases, the deposits were quite dense, showing little, if any, porosity.

C. *Crystal Structure Determination*

The electron diffraction patterns from the Al-Ti alloys, 7 to 10 patterns per sample, were all indexed as either face-centered cubic (fcc) or the ordered $L1_2$ crystal structure with $a_0 \approx 0.404$ nm. Examples of [001] zone axis diffraction patterns are shown in Figure 4, along with a labeled schematic. All of the deposits have intense 200 and 220 (and higher order) spots which form a square grid. The 100 reflections are not visible for alloy A (3.6Ti) but are observed in the other binary alloys. These superlattice reflections grow progressively more intense relative to the 200 spots as the titanium concentration is increased. The presence of superlattice reflections indicates that the crystal structure of the higher titanium deposits is not disordered fcc, since the 100 and 110 reflections are forbidden in fcc crystals due to the structure factor, as will be discussed subsequently. There was no evidence of the equilibrium $D0_{22}$ Al_3Ti phase (body-centered tetragonal, $a_0 = 0.384$ nm and $c_0 = 0.858$ nm) in any of the diffraction patterns or the high-temperature variant Ti_8Al_{24} identified by van Loo and Rieck[19] (tetragonal, $a_0 = 0.388$ nm and $c_0 = 3.384$ nm).

The electrodeposits are all single phase based on the observation that all dark-field micrographs using either fundamental or superlattice reflections completely illuminated the selected grain. This uniform illumination indicates that the superlattice reflections did not originate from coherent $L1_2$ precipitates. Lattice imaging of {100} planes was also used in the 24.1Ti specimen to determine if any disordered regions (where {100} planes would not be imaged) were present (Figure 5). The images of the planes are continuous and show no evidence of curvature. Lattice images of {111}-type planes in specimen B (5.3Ti) also indicated the absence of precipitates, although ordered and disordered regions would appear the same using this reflection.

D. *Growth Morphology*

1. *Low titanium deposits*

The growth morphology of the 3.6 and 5.4 at. pct Ti deposits is shown in Figure 6. The grains of these deposits are elongated in the growth direction which is normal to the substrate; this growth morphology is analogous to a columnar zone in a casting. Two twin variants are clearly visible in the micrograph of the 3.6Ti specimen. Growth striations, which are parallel to {111} planes, are more readily visible at higher magnifications (Figure 7). The striations cannot be due to fine, regular twins, since electron diffraction patterns from multiple striations are indexed as single crystals rather than twin-related single crystals. Another possible cause of the striation contrast, thickness fringes, can be dismissed, since the thickness of the specimens was extremely uniform, based on the observed electron transparencies. Further evidence against thickness fringes is the sharp change in striation orientation across grain boundaries, as was shown in Figure 6(b). Compositional differences were not observed between the striations and the striation boundaries by TEM/EDS. However, the data gathered do not provide conclusive evidence that compositional differences do not exist and, in fact, the striation contrast is most likely caused by compositional variations which are below the spatial resolution and counting statistics limitations of TEM/EDS.

The grains of the low titanium deposits are heavily twinned, particularly during the initial stages of growth from the copper substrate. An example where two {111} twin variants are visible at the deposit/substrate interface is shown in Figure 6(a). A [011] zone axis diffraction pattern from both sides of a twin boundary is shown in Figure 8(a). The growth of the nodules is also related to the presence of the {111} twins. A low magnification view of a nodule is shown in Figure 8(b). The twin plane runs through the center of the nodule and is parallel to the apparent growth direction. Figure 8(c) shows a high magnification view of a typical nodule bisected by a twin boundary. The sides of the nodule are parallel to the growth striations and are sharply faceted. The angles between the striations and the twin boundary (which is

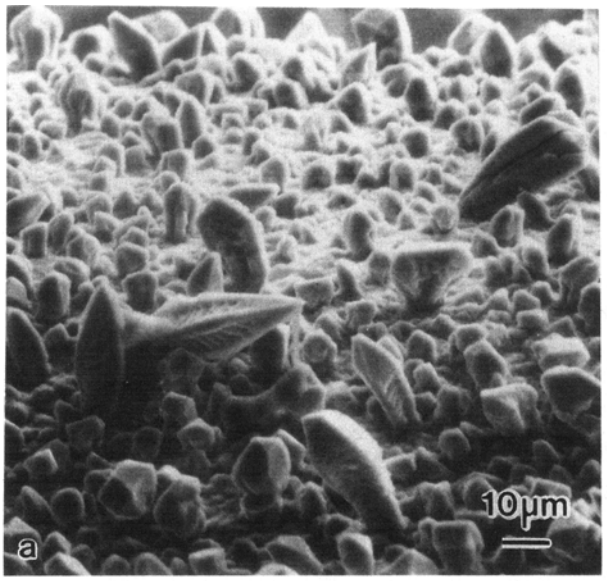

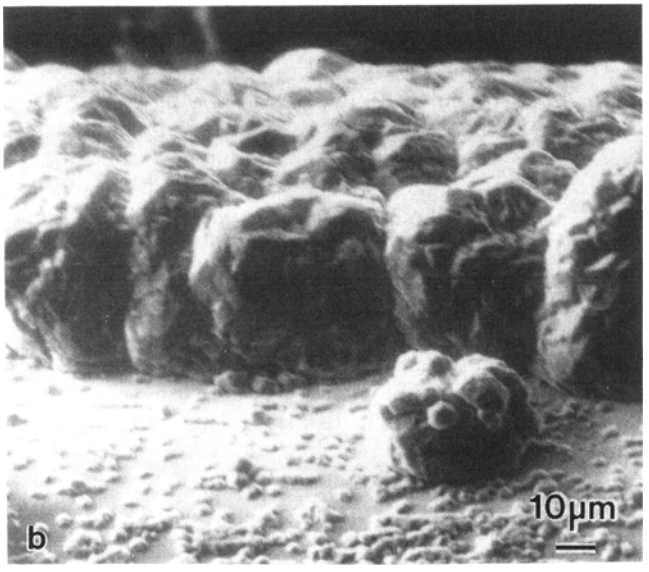

Fig. 3—Scanning electron micrographs showing the surface morphology of specimens (*a*) A (3.6Ti) and (*b*) D (24.1Ti).

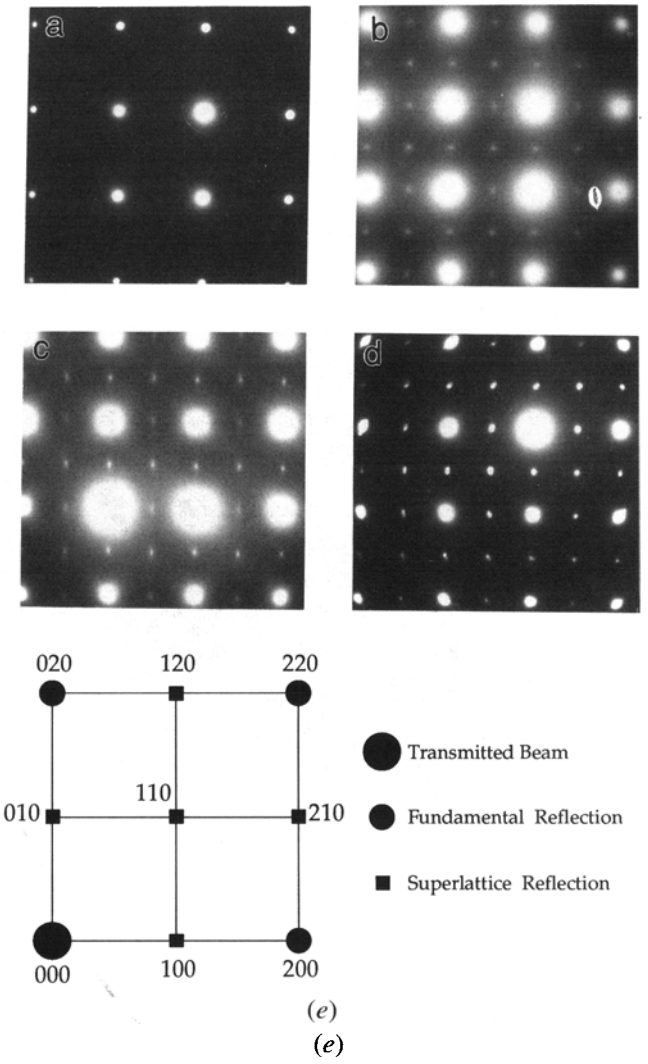

Fig. 4—Selected area diffraction patterns taken on the [001] zone axis which shows the increasing relative intensity of the superlattice reflections with increasing Ti content: (*a*) 3.6Ti; (*b*) 5.3Ti; (*c*) 15.8Ti; and (*d*) 24.1Ti. A labeled schematic of the diffraction pattern is shown in (*e*).

slightly inclined to the electron beam in this micrograph) are between 65 and 75 deg. These angles were measured from six different nodules and are consistent with the angle between any two nonparallel {111} planes. The measurements are within measurement error of a cubic crystal, for which the theoretical value is 70.5 deg. The angular data indicate that the growth of the nodules occurs by the addition of successive {111} planes which meet at a {111} twin plane. However, the twin planes are not microscopically planar but have numerous steps, which can be seen in Figure 7.

2. *High titanium deposits*

The grain structure of the deposits with high titanium contents (designated C and D) is also columnar; some {111} twins are also present. The columnar grains can be seen in the (200) dark-field micrograph of Figure 9(a) (alloy C). Note that nearby grains are partially illuminated, which indicates that the grains have nearly the

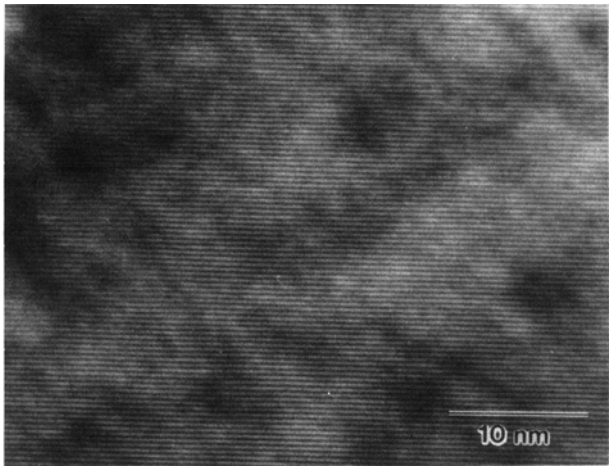

Fig. 5—Lattice images of a set of {100} planes in the 24.1Ti specimen.

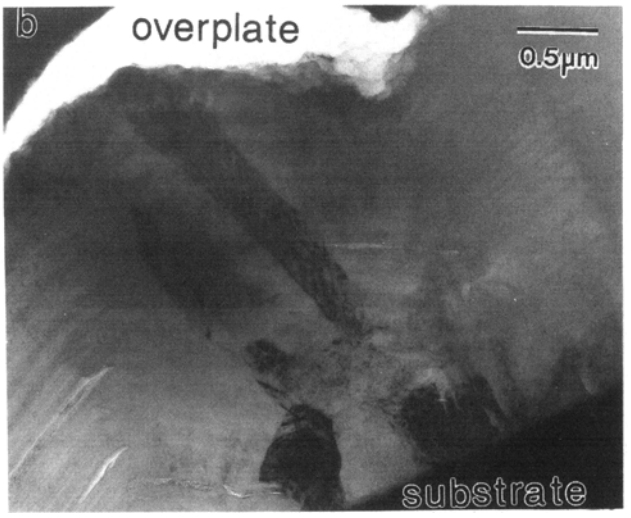

Fig. 6—Transmission electron micrographs of the (*a*) 3.6 and (*b*) 5.3 Ti specimens. The copper substrate and overplating are labeled when shown. Two {111} twin variants are visible in (a), and columnar grains and growth striations are evident in (b). These features are typical of both low Ti deposits.

same orientation. In contrast to the low titanium deposits, growth striations are not evident in alloys C and D. The grains in the 15.8 and 24.1Ti specimens have a great deal of internal structure, as can be seen in Figures 9(b) and (c). Due to the extremely fine grain size of these specimens, it was not possible to do the systematic tilting experiments necessary to identify the internal structure which led to this contrast. The identification of the internal grain structure will likely be an area of study in the future.

IV. DISCUSSION

The Al-Ti phase diagram information presented in References 20 and 21 indicates that (1) Ti has a low solubility in aluminum (≈0.7 to 0.8 at. pct at 660 °C) which rapidly decreases at lower temperatures (≈0.4 at. pct at 550 °C) and (2) the line compound Al_3Ti ($D0_{22}$)

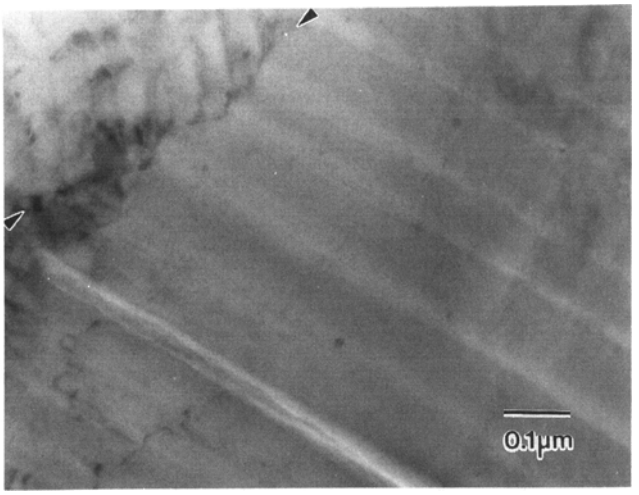

Fig. 7—Transmission electron micrograph of growth striations in a nodule. In this example from the 5.3Ti deposit, the twin boundary which bisects the nodule is marked with arrows.

is the next phase in order of increasing Ti content. Thus, the equilibrium structure of the deposits of this study (3.6 to 24.1Ti) is two phase: fcc Al (saturated with Ti) and $D0_{22}$ Al_3Ti. Therefore, the structures observed in this study are nonequilibrium in two senses: (1) they are single phase and (2) the crystalline phase is $L1_2$ (rather than $D0_{22}$). The latter result is not surprising, because small amounts of transition elements have been found to change the equilibrium structure of Al_3Ti-based alloys from $D0_{22}$ to $L1_2$, which suggests that there is a very small difference in free energy between the two phases. Fu[22] showed that the energy difference between binary Al_3Ti in the two crystal structures $L1_2$ and $D0_{22}$ is quite small, about 0.025 eV/atom. For comparison, the energy for the $\alpha \rightarrow \beta$ phase transition in pure Ti is about 0.04 eV.[23] The magnitude of the energy difference between Al_3Ti in the $L1_2$ and $D0_{22}$ structures suggests that it should be possible to form $L1_2$ Al_3Ti in a binary alloy, as was done in this study.

Metastable or unstable structures are formed by raising the free energy of the starting materials and then removing that energy rapidly enough to ensure that the atomic mobility is sufficiently low to prevent or limit subsequent transformations.[24] The many fabrication processes which allow one to maintain these structures can generally be divided into three categories: quenching, molecular deposition, and external action (deformation, irradiation, or chemical attack).[25] In rapid solidification, the cooling rate is primarily a function of the smallest dimension of the sample and the medium used to remove the heat. Unless an amorphous phase is retained, nucleation seems to limit the degree of supercooling to about 30 pct of the melting temperature; *i.e.*, $\Delta T/T_m \approx 0.3$.[26] Based on this limitation, it is generally impossible to produce a metastable crystalline phase from the melt having an excess free energy relative to the equilibrium form larger than ~0.3 ΔH_m (~0.03 eV), where ΔH_m is the enthalpy of melting.[27,28] The fact that the $L1_2$ phase has not been observed in rapidly solidified binary alloys[29,30] is most probably due to the fact that the energy difference between the $L1_2$ and $D0_{22}$ crystal

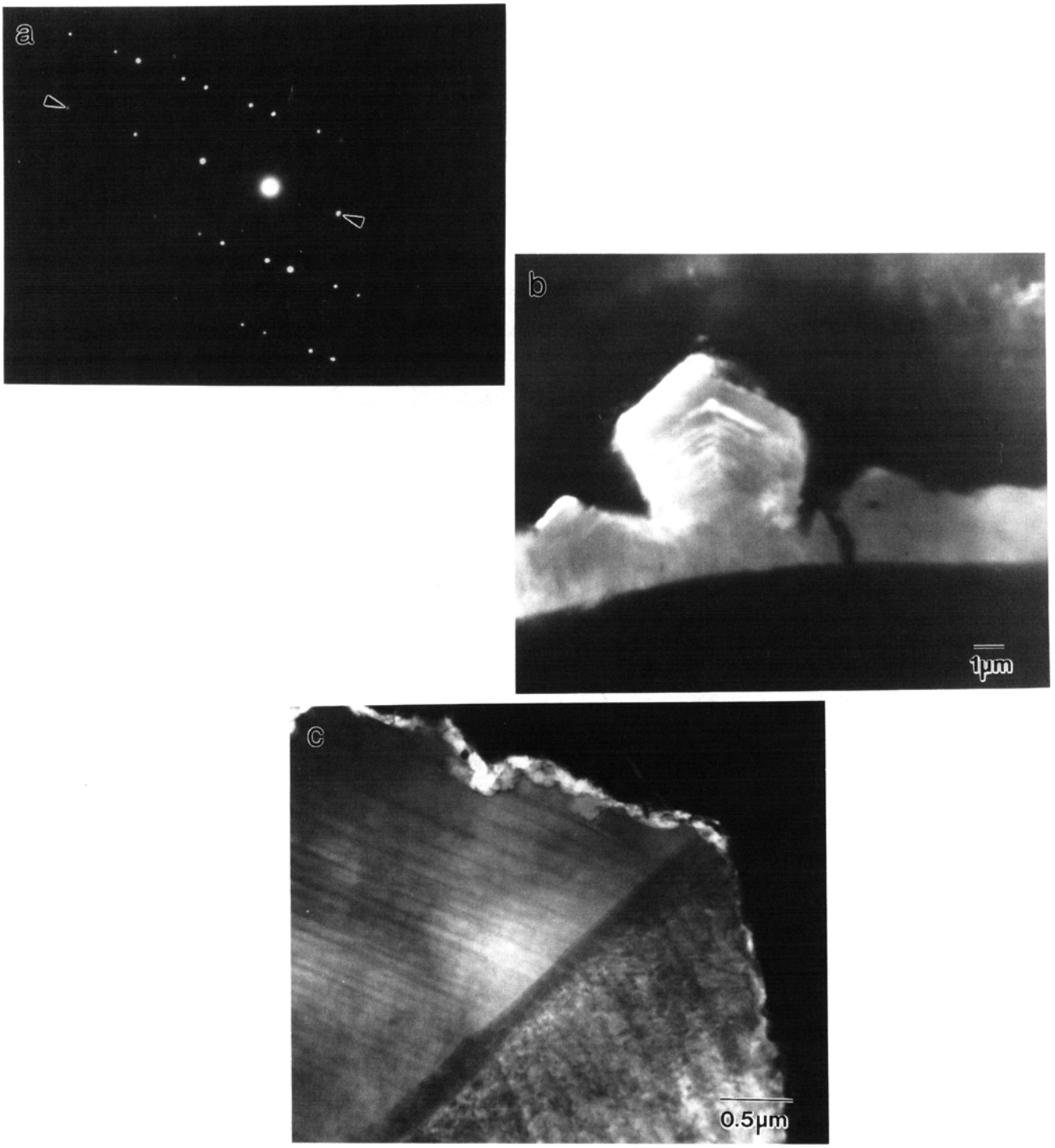

Fig. 8—Selected area diffraction pattern and electron micrographs of twinned regions in low Ti specimens. From the 3.6Ti deposit, a [011] zone axis diffraction pattern with the twin plane marked is shown in (*a*) Low and high magnification views of twinned nodules in the 5.3Ti deposit are shown in (*b*) and (*c*), respectively.

structures (0.025 eV) approaches the excess free energy limit of this technique (0.03 eV).

In condensation, vapor deposition, or sputtering, the extent of supercooling possible is much greater than that from the melt. In addition, the enthalpy of vaporization is generally an order of magnitude larger than that of melting. Consequently, one can produce metastable crystalline phases having an excess free energy on the order of ~0.5 eV, making vapor condensation a potentially much more powerful method for crystalline phase retention than melt solidification.[27,28] While exact correlations between electrodeposition and vapor deposition

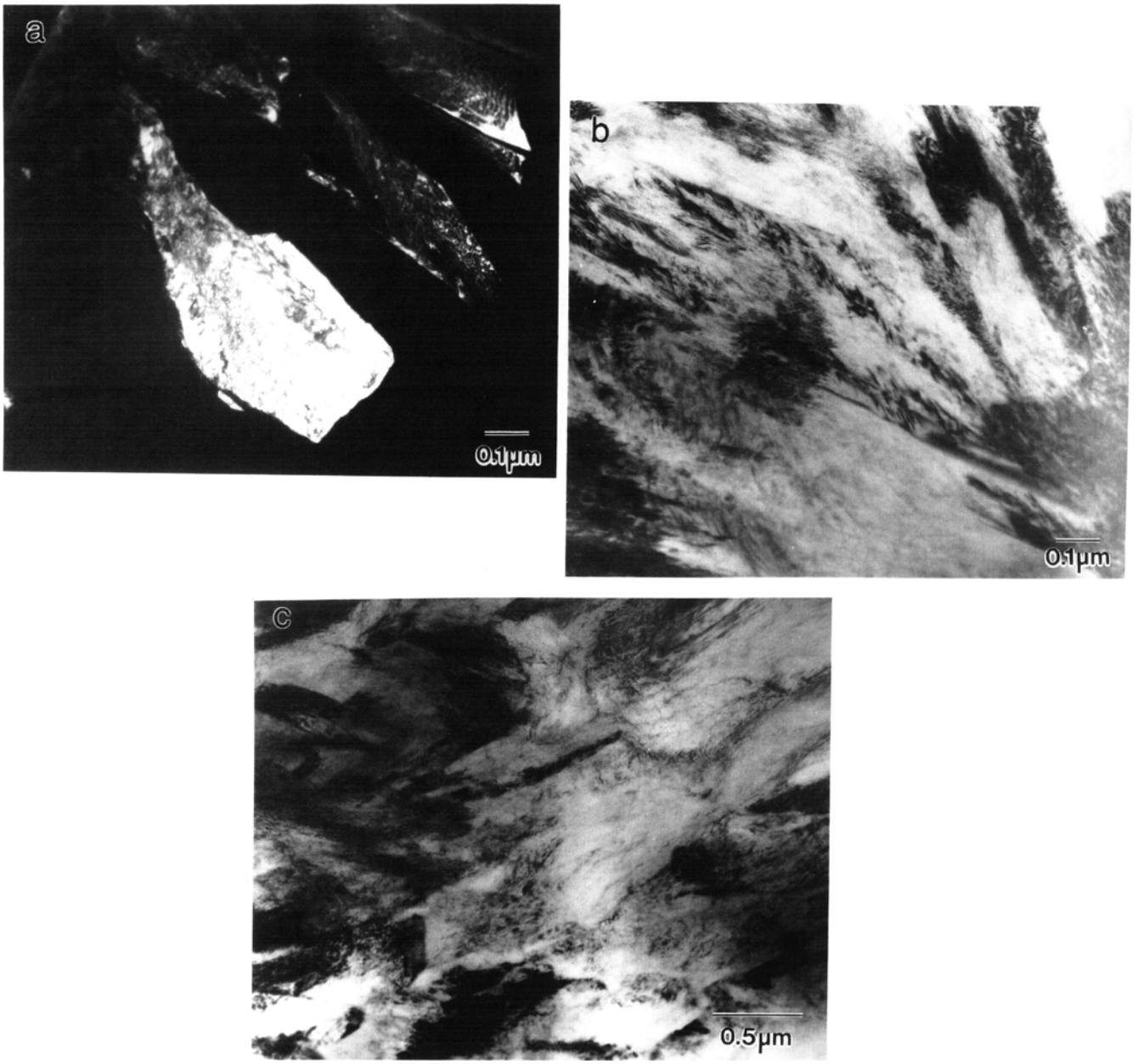

Fig. 9—Electron micrographs of the high Ti deposits. A dark-field micrograph of alloy C(15.8 Ti) using a (200) reflection which demonstrates the columnar nature of these deposits is shown in (*a*). The internal grain structure of the high titanium deposits is illustrated in (*b*) 15.8Ti and (*c*) 24.1Ti.

have not been developed, the excess free energy possible in alloys produced by these two techniques is similar.[27,31]

The presence of coherent twin boundaries throughout the deposits, and particularly at the corners of nodules, suggests that the twins play a significant role in deposit growth. This hypothesis is consistent with the solidification behavior of materials with high entropies of melting, where liquid/solid interfaces are atomically flat and require ledge motion to grow.[32] Potential sources of ledges include surface nucleation sites (above the critical size), screw dislocations, and twin intersections;[32] the latter two sites are permanent sources, since they are not consumed by the ledge growth. Since twins were not observed in pure electrodeposited Al, their occurrence may be the result of a reduction in the stacking fault energies due to the presence of titanium or a change in crystal structure, *i.e.*, ordering.

The morphology of the nodules suggests the manner by which the twins affect deposit growth. A schematic of a growth process which is consistent with the observations of this study is shown in Figure 10. The twin acts as a source of ledges,[32] and the striations, which are parallel to the {111} planes, emanate from the twin plane. Growth by {111} planes is consistent with the solidification of materials with high entropies of melting, where the growth plane is a close-packed plane.

The electron diffraction intensity data can be interpreted by considering the structure factors (also known

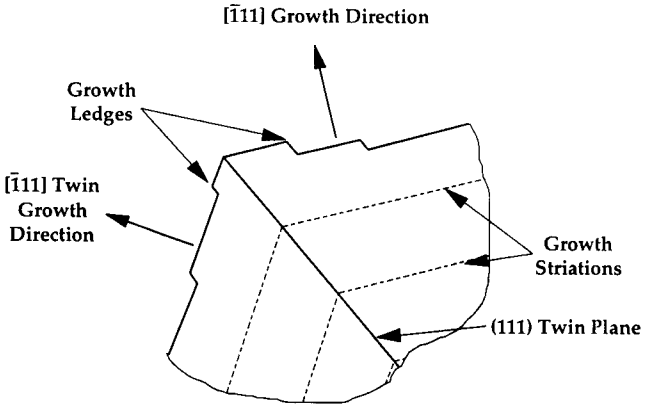

Fig. 10—Schematic of the proposed growth mechanism for twinned nodules.

as the form factors) of the fcc and $L1_2$ crystal structures. The structure factors for Al_3Ti with the $L1_2$ and fcc crystal structures are

$$I \propto F^2 = (3f_{Al} + f_{Ti})^2 \text{ for fundamental reflections (fcc and } L1_2)$$

$$I \propto F^2 = (f_{Al} - f_{Ti})^2 \text{ for superlattice reflections } (L1_2)$$

$$I \propto F^2 = 0 \text{ for superlattice reflections (fcc)}$$

where I is the intensity of a given reflection, F^2 is the structure factor, f_{Al} is the scattering factor for the Al lattice sites, and f_{Ti} is the scattering factor for the Ti lattice sites. The scattering factor for a lattice site is the weighted average of the atomic scattering factors of the atoms that occupy it. Since some of the titanium lattice sites must be occupied by aluminum atoms in the substoichiometric alloys (assuming all lattice sites are occupied), the difference in the scattering factors for the two sites and, therefore, the superlattice reflection intensities must decrease. A plot of the relative intensities of the 100 and 200 reflections and their ratios as a function of Ti content is shown in Figure 11. The scattering factor data were taken from Reference 33. As was expected, the intensity of the superlattice reflections decreases significantly as the Ti content is reduced. This prediction is in qualitative agreement with the experimental observations. It is not possible to ascertain if the apparent absence of superlattice reflections in the 3.6Ti specimen is due to low intensity or to a disordered crystal structure because of the loss of superlattice reflection intensity at low Ti concentrations. However, the maximum equilibrium solubility of Ti in Al has been exceeded by a factor of 4 in the 3.6Ti specimen. Thus, it is in a nonequilibrium state whether its structure is nonstoichiometric $L1_2$ or supersaturated fcc.

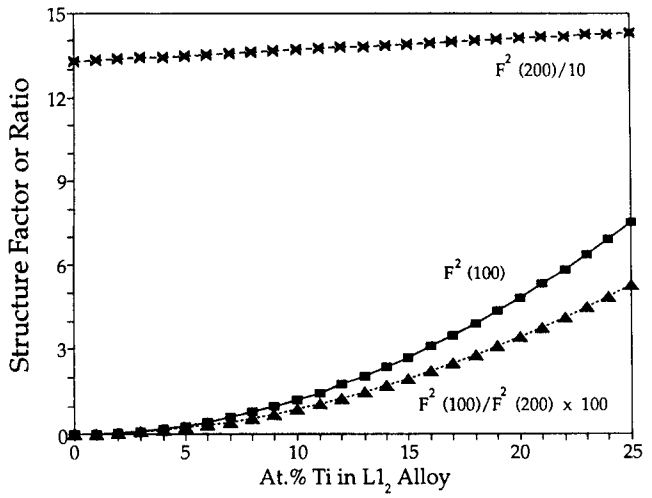

Fig. 11—Structure factor and structure factor ratios for (100) and (200) reflections from an Al_3Ti-based $L1_2$ crystal as a function of titanium content.

V. SUMMARY/CONCLUSIONS

1. Al_3Ti-based alloys with between 3.6 and 24.1 at. pct Ti can be fabricated by electrodeposition from chloroaluminate electrolytes containing Ti^{+2}.
2. The presence of growth striations (with ⟨111⟩ normals) and {111} twins suggests a growth mechanism where the twins act as ledge sources.
3. The electron diffraction patterns indicate that the crystal structure of the deposits is fcc for 3.6Ti and $L1_2$ for 5.3, 15.8, and 24.1 Ti. All deposits are single phase. It is possible that the 3.6Ti deposit also has the $L1_2$ crystal structure but that the superlattice reflection intensity is too low due to the small differences in the composition of the two lattice sites.

ACKNOWLEDGMENTS

The principal support for this project was from the Office of Naval Research, Dr. Steven Fishman, Contract Monitor. The support for GMJ was a National Research Council/National Institute of Standards and Technology Postdoctoral Associateship. The technical expertise of Dr. David Lashmore and Dr. Alexander Shapiro and the assistance of Ms. Sandra Claggett and Ms. Shari Tobery are also gratefully acknowledged.

REFERENCES

1. W.O. Powers and J.A. Wert: *Metall. Trans. A*, 1990, vol. 21A, pp. 145-51.
2. Hiroshi Mabuchi, Ken-ichi Hirukawa, and Yutaka Nakayama: *Scripta Metall.*, 1989, vol. 23, pp. 1761-66.
3. J.P. Nic, S. Zhang, and D.E. Mikkola: *Scripta Metall.*, 1990, vol. 24, pp. 1099-1104.
4. S. Zhang, J.P. Nic, and D.E. Mikkola: *Scripta Metall.*, 1990, vol. 24, pp. 57-62.
5. E.P. George, J.A. Horton, W.D. Porter, and J.H. Schneibel: *J. Mater. Res.*, 1990, vol. 5 (5), pp. 1639-48.
6. J. Tarnacki and Y.-W. Kim: *Scripta Metall.*, 1988, vol. 22, pp. 329-34.
7. K.S. Kumar and J.R. Pickens: *Scripta Metall.*, 1988, vol. 22, pp. 1015-18.
8. A. Raman and K. Schubert: *Z. Metallkd.*, 1965, vol. 56, pp. 99-104.
9. Benjamin Grushko and Gery R. Stafford: *Scripta Metall.*, 1989, vol. 23, pp. 557-62.
10. B. Grushko and G.R. Stafford: *Metall. Trans. A*, 1989, vol. 20A, pp. 1351-59.
11. B. Grushko and G.R. Stafford: *Metall. Trans. A*, 1990, vol. 21A, pp. 2869-79.
12. G.R. Stafford: *J. Electrochem. Soc.*, 1989, vol. 136, pp. 635-37.

13. B. Grushko and G.R. Stafford: *Scripta Metall.*, 1989, vol. 23, pp. 1043-48.
14. G.R. Stafford: National Institute of Standards and Technology, Gaithersburg, MD, unpublished research, 1991.
15. J. Bouteillon and A. Marguier: *Surface Technology*, 1984, vol. 22, pp. 205-17.
16. B. Nayak and M.M. Misra: *J. Appl. Electrochem.*, 1977, vol. 7, pp. 45-50.
17. B. Nayak and M.M. Misra: *J. Appl. Electrochem.*, 1979, vol. 9, pp. 699-706.
18. R.C. Howie and D.W. Macmillan: *J. Appl. Electrochem.*, 1972, vol. 2, pp. 217-22.
19. F.J.J. van Loo and G.D. Rieck: *Acta Metall.*, 1973, vol. 21, pp. 61-71.
20. Yoritoshi Minamino, Toshimi Yamane, Hideki Araki, Naoya Takeuchi, Yan-Sheng Kang, Yoshinari Miyamoto, and Taira Okamoto: *Metall. Trans. A*, 1991, vol. 22A, pp. 783-84.
21. J.L. Murray: in *Binary Alloy Phase Diagrams*, 2nd ed., Thaddeus B. Massalski, Hiroaki Okamoto, P.R. Subramanian, and Linda Kacprak, eds., ASM INTERNATIONAL, Metals Park, OH, 1990, pp. 225-27.
22. C.L. Fu: *J. Mater. Res.*, 1990, vol. 5 (5), pp. 971-79.
23. *Handbook of Chemistry and Physics*, 61st ed., Robert C. Weast, ed., Chemical Rubber Company, Boca Raton, FL, 1980–1981, p. D-63.
24. F. Spaepen: *Science*, 1987, vol. 235, pp. 1010-14.
25. H. Jones: in *Proc. 2nd Int. Conf. on Rapidly Quenched Metals*, B.C. Giessen and N.J. Grant, eds., MIT Press, Cambridge, MA, 1976, pp. 1-27.
26. J.H. Hollomon and D. Turnbull: *Prog. Metall. Phys.*, 1953, vol. 4, pp. 333-88.
27. J.C. Baker and J.W. Cahn: *Thermodynamics of Solidification*, ASM, Metals Park, OH, 1971, pp. 23-58.
28. A.K. Sinha, B.C. Giessen, and D.E. Polk: *Crystalline and Noncrystalline Solids*, Treatise on Solid State Chemistry, 1976, vol. 3, pp. 1-88.
29. T. Hanamura, T. Sugai, and M. Tanino: *J. Mater. Sci.*, 1990, vol. 25, pp. 3286-90.
30. E.L. Hall and Shyh-Chin Huang: *Acta Metall. Mater.*, 1990, vol. 38, pp. 539-49.
31. Donald E. Polk and Bill C. Giessen: in *Metallic Glasses*, ASM, Metals Park, OH, 1978, pp. 1-16.
32. D.A. Porter and K.E. Easterling: *Phase Transformations in Metals and Alloys*, Van Nostrand Reinhold Co., Ltd., Berkshire, England, 1982, pp. 202-03.
33. P. Hirsch, A. Howie, R.B. Nicholson, D.W. Pashley, and M.J. Whelan: *Electron Microscopy of Thin Crystals*, 2nd revised ed., R.E. Krieger Publishing Co., Inc., Malabar, FL, 1977, pp. 504-05.